 doi:10.20944/preprints202208.0092.v1

Article

Numerical Simulation and Characterization of the Hydrogeomechanical Alterations at the Zafarraya Fault Due to the 1884 Andalusia (Spain) Earthquake

Manuel Mudarra-Hernández[1]*, Juan Carlos Mosquera-Feijoo[2]* and Eugenio Sanz-Pérez[3]

[1] ETSI Caminos, Canales y Puertos, Universidad Politécnica de Madrid (Spain), manuel.mudarra.hernandez@gmail.com
[2] ETSI Caminos, Canales y Puertos, Universidad Politécnica de Madrid (Spain), juancarlos.mosquera@upm.es
[3] ETSI Caminos, Canales y Puertos, Universidad Politécnica de Madrid (Spain), eugenio.sanz@upm.es
* Correspondence: manuel.mudarra.hernandez@gmail.com (M.M-H.); juancarlos.mosquera@upm.es (J.C.M-F.)

Abstract: The 1884 Andalusia Earthquake, with an estimated Magnitude between 6.2 and 6.7, is one of the most destructive events that shook the Iberian Peninsula, causing around 1200 casualties. According to both paleoseismology studies and intensity maps, the earthquake source relates to the normal Ventas de Zafarraya Fault (Granada, Spain). Diverse hydrological effects were registered and later studied: landslides, rockfalls, soil liquefaction, all-around surge and loss of springs, alterations in the phreatic level, discharge in springs and brooks, and well levels, along with changes in water properties. Further insight into these phenomena found an interplay between hydro-geomechanical processes and crust surface deformations, conditions, and properties.

This study focuses on simulating the features involved by the major 1884 event and aims at elucidating the mechanisms concerning the mentioned effects. It encompasses conceptual geological and kinematic models, and a 2D finite element simulation to account for the processes undergone by the Zafarraya Fault. The study focuses on the variability of hydro-geomechanical features and the time evolution of the ground pore-pressure distribution in both the preseismic and coseismic stages, matching some of the shreds of evidence found by field studies.

This methodology can be applied to other events registered in the National Catalogues of Earthquakes to reach a deeper insight, further knowledge, and better understanding of past earthquakes.

Keywords: hydrogeological effects; hydro-geomechanical modelling; Andalusia 1884 Earthquake; pore pressure effects; poroelasticity and seismicity

1. Introduction

The 1884 Andalusia Earthquake is one of the most destructive events that shook the Iberian Peninsula, involved around 1200 casualties, twice injured victims, destroyed some 14000 homes and damaged other 13000 ones [1]. The tremor lasted around ten seconds, with an estimated Mw between 6.2 and 6.7 on the Richter scale, and had its focus between 10 and 20 km depth [2-4]. Diverse aftershocks followed the main shock during the very later days, some of them with rather notable intensity.

The 1884 earthquake was felt in an area of 120 x 70 km^2, affecting about one hundred urban centers in the provinces of Granada and Malaga. The most affected areas, with significant building collapses, deaths and injuries, were the Southwest of the province of Granada and the East of the province of Malaga. Arenas del Rey was the most affected population: 90% of the houses collapsed, the rest suffered damages; 135 dead and 253 wounded people. This town was later rebuilt in the current location, a few kilometers away from the previous one. Alhama de Granada underwent the highest number of vic-

 doi:10.20944/preprints202208.0092.v1

tims, 463 dead and 473 injured. More than 70% of the houses collapsed. Then a new quarter was built near the Hoya del Ejido. After the 1754 Lisbon earthquake, the only quake in the Iberian Peninsula with greater magnitude than the 1884 event occurred in 1954, with its epicenter in Granada. However, the destruction in this case was not as great. The tremor caused rock falls and landslides on slopes, aggravating the earthquake effects. The former also caused the formation of numerous cracks. In addition, the earthquake induced hydrogeological effects of diverse ranges [5-7].

On January 7, 1884, the Spanish Government appointed a committee to study the earthquake led by the mining engineer Manuel Fernández de Castro y Suero (1825-1895). They immediately visited the region and distributed a 33-question survey including several queries about the alteration of sources, wells, rivers, etc. The French Academy of Sciences sent another commission, and so did the Italian Government and the Academia dei Lincei, who sent seismologists Torquato Taramelli and Giuseppe Mercalli, who also provided an extensive report on the geology of the area with a map of the shake intensity. The geologist José Macpherson y Hemas (1839-1902) explained that the earthquake mechanism was the movement along the faults that joined the Tejeda/Almijara massif to the North and South.

According to the most recent seismotectonic studies, the source of this earthquake is associated with the gravity fault of Ventas de Zafarraya (Granada, Spain). The trench study, to which the isosists are also adjusted, has evidenced such a source (Figure 1) [5]. During the recent Tertiary and Quaternary, the fault activity has entailed the subsidence of the area and the formation of a small and elongated graben, which in turn has originated the so-called Polje de Zafarraya. This polje is located in the southwest of the Granada Depression, is bordered to the N with the calcareous reliefs of Sierra Gorda and to the S with those of Sierra de Alhama. The polje borders on the SE with the metamorphic materials of Sierra Tejeda, so it lies in the contact between the external and internal regions of the Betic Range (Figure 1). Earlier studies reveal that the water table rose on the NNW side of the Zafarraya Fault and declined on the SSE region.

Further insight into these phenomena sheds light on the interplay between hydro-geomechanical processes and crust surface deformations, i.e., interaction among the water cycle, the tectonic layout conditions, and the crustal geomechanical properties.

Furthermore, the hydrogeological effects of the interaction between groundwater and earthquakes include soil liquefaction, mud volcanoes, geysers, all-around surge and loss of springs, increased discharge in springs and streams, changes in the physical and chemical properties of groundwater or its pressure distribution [8, 9]. As known, the hydrological variations due to earthquakes can affect several hundred kilometers around, and the processes can even last for months or years. These phenomena result from the interaction among hydrogeological processes, mechanical properties, and tectonic characteristics of the earth's crust due to earthquake-induced deformations. An earthquake causes changes in the stress state of the crust, decreasing with distance. Most of these hydrological alterations appear during and after the earthquake, and only in very few cases can they be foreshocks signs.

This earthquake also provoked numerous hydrogeological alterations that we have been able to collect. Despite the limited availability of quantified data on this historical earthquake, dated more than a century ago, the tectonically earthquake-induced fluid flows may have notable implications for our understanding of the kinematic behavior of the assumed source fault.

Thus, the objectives of this work are the following:

- Description and analysis of the hydrogeological phenomena induced by the Andalusian earthquake of 1884.
- Establishment of a hydro-geomechanical conceptual model of the Zafarraya fault that explains and allows understanding of these hydrological alterations.
- Implementation of a hydro-geomechanical numerical model to simulate the conditions of the massif surrounding the main fault during the pre-seismic and co-seismic

 doi:10.20944/preprints202208.0092.v1

phases. The results obtained from this simulation allow us to understand and explain the features and effects of the 1884 major event.

- Perform a matching and validation of both models.

This study focuses on simulating the hydro-geomechanical features involved by the 1884 Andalusia Earthquake and aims at elucidating the mechanisms that caused the mentioned effects. Then it encompasses a conceptual geological model, a kinematic one, and a numerical simulation procedure to account for the processes undergone by the Zafarraya Fault because of the major 1884 event. The former comprises a 60-degree average northward dip with a ten-kilometer-away outcrop level and a blind fault thrusting from SSE, causing a ground rise in Sierra Tejada and a normal subsidence fault on the NNW side and hence a graben formation, namely the Zafarraya Polje [10-12].

The study attempts to elucidate the rationale behind the 1884 event through a set of 2D finite element simulation models to account for the variability of hydro-geomechanical features. This approach includes the coupling between poromechanical and hydrological constitutive behaviors of the ground surrounding the fault. The numerical model has undergone a preliminary calibration stage to account for the regional specific conditions. Its results allow one to explain the source of fault displacements and understand the time evolution of the pore pressure distribution that occurred during the 1884 event. Likewise, the numerical simulation allows one to meet with some of the shreds of evidence found by field studies.

This numerical simulation procedure can apply to other registered events in the National Catalogues of Earthquakes to grasp deeper insight, further knowledge, and a better understanding of past earthquakes.

2. Materials and Methods

2.1. Methodology

The methodology followed in this study comprises the following steps:

- Description of the hydrological alterations due to the 1884 Andalusia earthquake according to historical surveys.

  The information on the earthquake-induced hydrogeological alterations stems from four sources, which sometimes refer to the same water points by adding or complementing the information. These sources are Surveys of the Spanish National Geographic Institute (IGN), the Committee of the Geological Map of Spain of 1884, the work of Domingo de Orueta, and the Spanish Commission (1885).

  The IGN survey covered 66 towns (leaving aside farmhouses) in the provinces of Malaga, Granada, and Jaén. The Committee of the Geological Map of Spain refers to the alterations in the 11 most affected counties and towns. Seven of the most affected counties and villages appear in Domingo de Orueta's work. In addition, the Spanish Committee's document described the alterations that occurred as well. Despite a long time, the surveys are rather extensive and offer reliability as it has been possible to carry out a quantitative analysis by relating them to the current geological and hydrogeological information about the region.

- Based on bibliographic background, the next stage seeks the setup of the geological and hydrogeological framework, and the seismotectonic characterization of the Zafarraya Fault surrounding area.
- Setup of a preliminary hydro-geomechanical conceptual model.
- The next stage involves the setup of a hydro-geomechanical 2D finite element plane-deformation model built on the conceptual one. Such a model accounts for the fully coupled phenomenon, i.e., the interplay among the fault friction, the existence of interstitial water in the pores, and a poro-viscoelastic medium. The ground is assumed homogeneous and isotropic, although it includes a heterogeneous initial stress field due to its tectonic history. The simulation considers the fault as a one-dimensional

 doi:10.20944/preprints202208.0092.v1

entity with a "slip-weakening" frictional response, i.e., its frictional resistance weakens when the relative slip between its edges is triggered [13]. Seismic rupture occurs when the acting tangential stresses reach the frictional resistance value at any part of the fault.

2.2. The Zafarraya fault: tectonic context, displacement and recurrence periods

This fault is located in the Betic Range and results from compressive and extensive deformations associated with the boundary between the Eurasian and African plates. The current average relative motion between both plates is 4 mm/year, which produces an oblique convergence in the NW-SE direction [14]. The study area belongs to the central-eastern sector of the Betic Range, whose current reliefs have evolved from the Tortonian to the present. The main structures identified in the region with recent tectonic activity are folds of kilometer size and E-W orientation, generally asymmetric and some with N vergence. Thus, these determine the formation of the main mountain ranges, such as Sierra Tejeda or Sierra Nevada. Besides, E-W and NW-SE orientation faults predominate in this sector, usually having a marked normal regime. In addition, the seismicity data indicate a main detachment level located between 10 and 20 km deep (Figure 1).

Field observations indicate that the over-15-km-long Zafarraya fault orientation varies between E-W, south of Zafarraya, and NW-SE, at the western end (Figure 1). The fault plane dips 60º -70º to the N, pitches 40º to the East (dextral-normal component), and shows several sets of normal striae. The total jump is several hundred meters and develops an endorheic basin, the Polje of Zafarraya, filled with sediments from the Tortonian to the present. This basin is asymmetric, with the depocenter displaced towards the fault zone.

On the southeast of the Zafarralla Fault, Sierra Tejeda shapes an antiform with a large E-W to ESE-WNW radius and a periclinal termination to the W. The development of the antiform has produced a positive relief parallel to the fold axis. The antiform southern flank is deformed due to SW-dipping WNW-ESE oriented faults (Type II faults), formed during the Neogene but without recent activity [15] (Figure 1). The geodetic network allows to quantify the current deformation in the Zafarraya Fault and the Sierra Tejeda Antiform.

Since the Middle Miocene, the simultaneous development and interplay between folds and faults developed. The presence of a detachment level with current seismicity, which approximately constitutes the fold compensation level, divides the crust into two blocks with diverse behavior (Figure 1). The crustal detachment activity is probably due to the NW-SE oblique shortening of the boundary between the Eurasian and African plates. The E-W oriented folds with N vergence could be related to the in-depth existence of oblique ramps or blind faults subparallel to the plate boundary and that it had a right-hand transpressive jump. The surface outcrop of normal faults subparallel to the fold axes, such as the Zafarraya fault, could be a consequence of the extension and collapse in the external arcs of the antiforms that constitute the main mountainous elevations.

Paleoseismic studies reveal that the recurrence intervals for earthquakes of M>6.5 are 2000-3000 years [16]. The mean minimum displacement of the fault is 0.17 mm/year for the post-Tortonian and 0.35 mm/year for the Holocene. New paleoseismic data, based on the analysis of fault trenches and radiometric dating, allow us to reconstruct the last 10000- year seismic history of the Ventas de Zafarraya fault segment. Such studies have identified four major paleoseismic events (c. 6.5 + 0.5 Ms) that can be considered as the maximum possible earthquake on this fault [17]. One of the main conclusions is that the average recurrence period of these "characteristic earthquakes" is around 2000 years. It is, therefore, one of the main active faults in southern Spain.

Preprints (www.preprints.org) | NOT PEER-REVIEWED | Posted: 3 August 2022 doi:10.20944/preprints202208.0092.v1

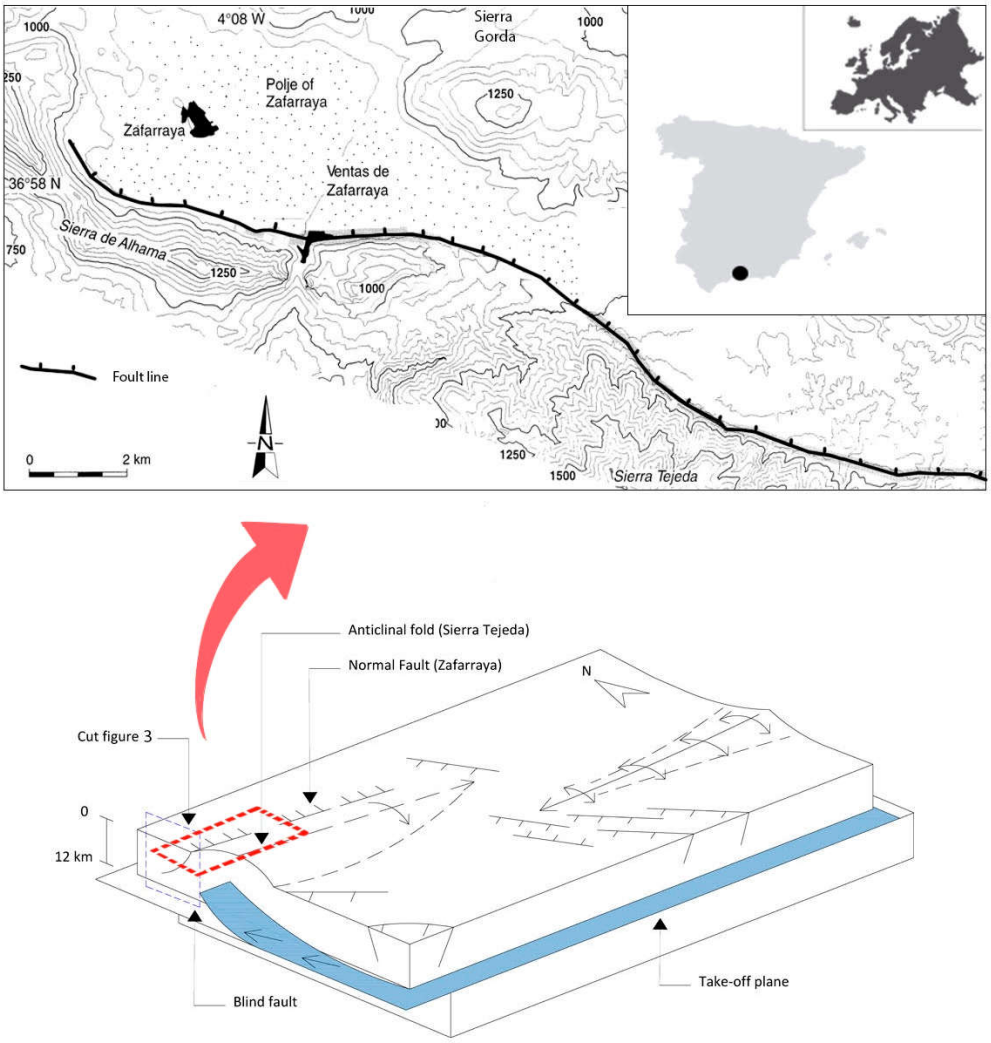

Figure 1. Above: location of the study area and trace of the Zafarraya Fault, source of the 1884 Andalusia earthquake (Adapted from [18]). Below: tectonic schematic of the simultaneous development of folds with possible blind thrust faults and two normal fault systems in a detachment roof block. Type I faults such as the Zafarraya Fault would be produced by external arc extension and collapse of the antiforms that constitute the main E-SW reliefs. Type II faults would respond to the regional stress field with a NE-SW extension direction. (Adapted from [15]).

The Polje of Zafarraya is an endorheic depression, which suffers periodic floods [19]. The polje is about 10 km long by 3.5 km wide, nearly flat and surrounded by large reliefs. It limits to the N with the calcareous reliefs of Sierra Gorda and to the S with those of Sierra de Alhama, whereas to the SE with the metamorphic materials of Sierra Tejeda. The polje is filled in its southern sector by materials from the Upper Miocene (calcarenite and marl) disposed on the subbetic substratum. The Quaternary fill is above the Miocene materials in the polje central part, while the western sector is directly above the Mesozoic. These Quaternary alluvial deposits feature two differentiated levels, the lower one being more clayey [20]. Jurassic carbonate rocks outcrop on the West bordered by normal faults. Likewise, loamy-clayey materials appear in the south of these outcrops, which can belong to either the Cretaceous-Paleocene materials of the Zafarraya unit or the Colmenar-Periana Complex [20].

The Polje of Zafarraya is limited mainly by normal faults, among which the Ventas de Zafarraya fault outstands. Although no fault outcrops on the northern edge, geophys-

Preprints (www.preprints.org) | NOT PEER-REVIEWED | Posted: 3 August 2022 doi:10.20944/preprints202208.0092.v1

ical studies and surveys suggest their existence. A recent gravimetric analysis has determined the basin sedimentary-infill geometric characteristics and identified some blind faults which fail to outcrop (Figure 1) [10].

Concerning hydrogeology, there are two aquifer systems in the area:

A. Sierra Gorda Karstic Aquifer: it holds a free aquifer with Jurassic limestone and dolomite and a Keuper impermeable bottom. The carbonate formations are more than 1000 m thick. The average rainfall in the area is 840 mm. Its hydrogeological parameters are T=40−16.4 $m2day$; S=me=1.5%.
B. Polje of Zafarraya detrital aquifer: Made up of Miocene and Quaternary infill sediments from the basin, having a maximum thickness of 280 m. The upper Miocene and Quaternary sediments are about 60 m thick and include sandy and gravel alluvial deposits with clay intercalations. In general, this upper detrital aquifer feeds the limestone aquifer underneath, but sometimes the reverse happens due to heavy rains that flood the polje. The flow is directed mainly towards the NE, with a gradient of 0.085-1.7%. This aquifer is heavily exploited, with 400 wells, and the water table is shallow, less than 15m deep.

2.3. Hydrogeological alterations: types and geographical distribution

Thanks to the Spanish National Geographic Institute surveys, the information provided in 1884 by the Committee of the Geological Map of Spain, and the reports of Domingo de Orueta and the Spanish Committee (1885), it has been possible to characterize the hydrogeological alterations produced by the earthquake. These encompass soil liquefaction (in Vélez-Málaga), the appearance of new springs, loss of existing springs and lowering of the water table (in Sierra Tejeda), persistent increase in discharge in springs and streams (the Alhama thermal spring), variations in well levels, in the physical and chemical properties of groundwater, in pressure [16, 21, 22].

Thus, the mentioned historical documentation states that the frequency and intensity of the alterations occurred around the epicentral area. Furthermore, the water table rose in the fault NNW near-field and broadly declined in the SSE region. Figure 2 depicts a schematic representation of the diverse hydrogeological alterations, the localities, and areas where these effects occurred.

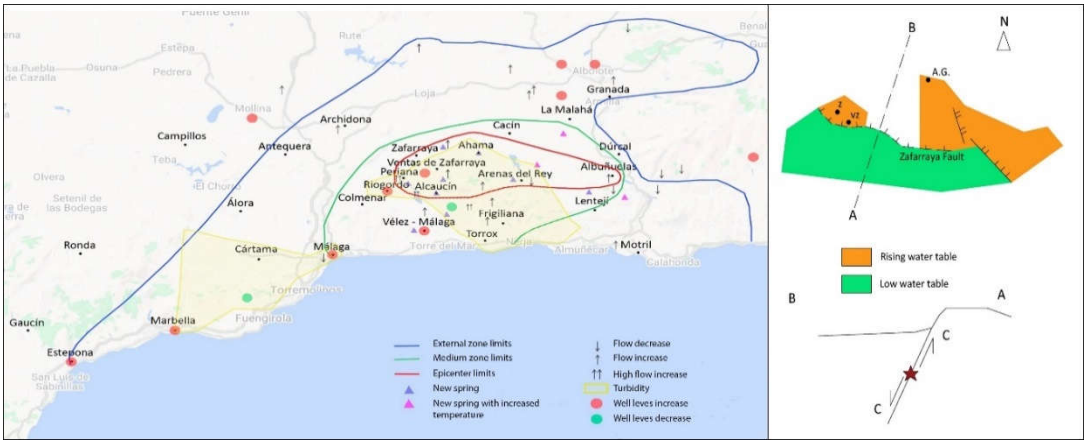

Figure 2. Alterations after the 1884 event. Left: map of the hydrogeological alterations produced. Right: Diagram of the variation of the phreatic level (Accronyms: Z, Zafarraya. VZ, Ventas de Zafarraya. A.G., Alhama de Granada).

2.4. 2D Geological model of the fault

The conceptual geological model represents the Zafarraya fault with a varying dip around 60º to the North, a detachment level 10 km away, and a blind thrust fault (Figure 3). The kinematic model depicts this blind fault pushing to the SSE, then producing an

Preprints (www.preprints.org) | NOT PEER-REVIEWED | Posted: 3 August 2022 doi:10.20944/preprints202208.0092.v1

uplift of Sierra Tejeda and consequently a normal subsidence fault to the NNW, with the formation of a graben, the Polje de Zafarraya [10-12].

Table 1 illustrates the parameters of the diverse grounds involved in this cut. A few geophysical works [10] and hydrogeology studies in this area [11] have supplied the data.

Table 1. Properties of the ground materials found in the 2D geological model.

	Density ρ_d (Ton/m³)	Effective porosity ϕ (%)	Permeability κ (m/s)	Depth of water table (m)
1	2.00	13	1 m/day	<15
2	2.00	10	10^{-4}-10^{-7}	-
3	2.00	0.5	10^{-6}	-
4	-	0.5	-	-
5	2.67	1.5	10^{-3}-10^{-9}	-
6	2.67	1.5	10^{-3}-10^{-9}	-

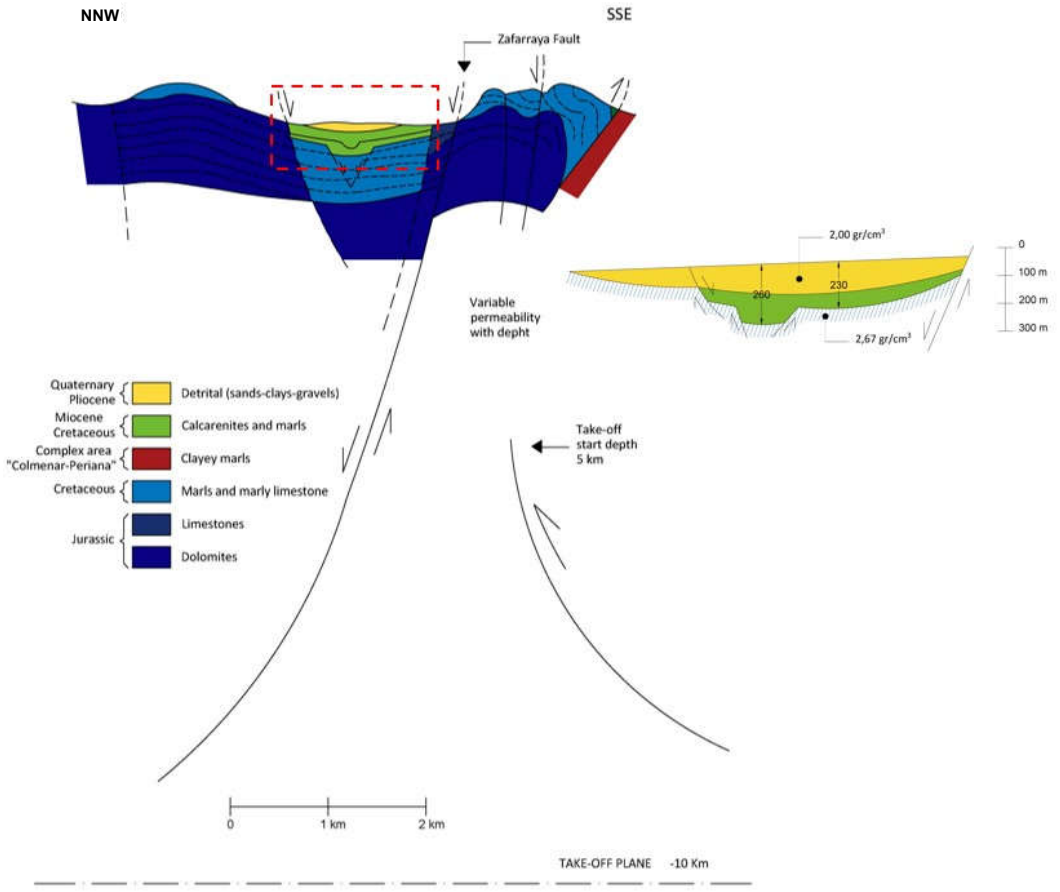

Figure 3. Above: Geological section of the Zafarraya fault. Bottom: Detail of the filling of the Zafarraya polje. (adapted from [10]).

Preprints (www.preprints.org) | NOT PEER-REVIEWED | Posted: 3 August 2022 doi:10.20944/preprints202208.0092.v1

2.5. Coupled physics included in the simulation model

The numerical analysis of the effects caused by earthquakes in the earth's crust needs to consider the coupling among the distinct physical processes involved: the fluid flow through the porous medium, the poromechanical ground response, and the fault frictional behavior. The procedure implemented here accounts for the interplay among those three physics (Figure 4). However, it becomes necessary to adopt assumptions and simplified formulations because of the complexity of the laws that govern each physical process.

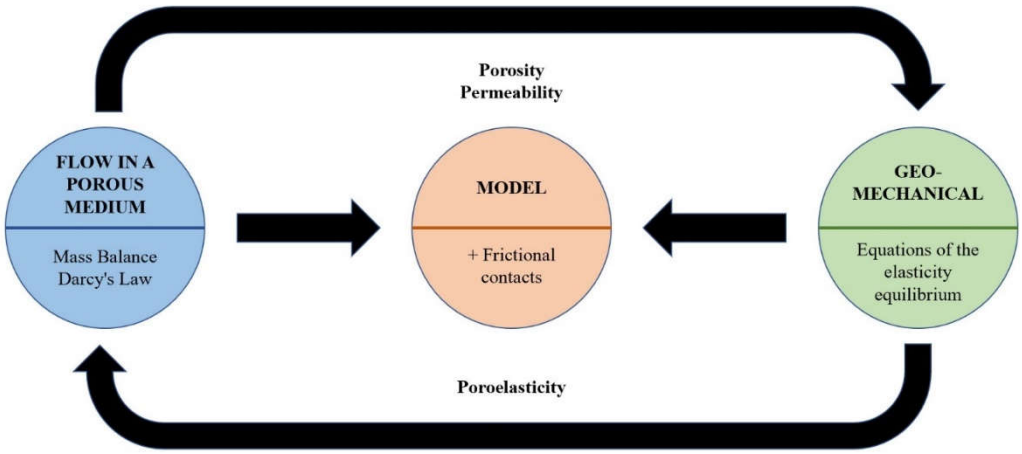

Figure 4. Schematic flowchart of the hydro-geomechanical coupling of the diverse physics involved in the numerical simulation.

The numerical simulation requires two types of discretization: time discretization and finite element assemblage. Likewise, the numerical solution of the equations governing the whole system response also requires a specific procedure, not to mention the time step variability suitable to search for the time response. The time solution procedure monolithically solves the values of the pore-fluid pressure evolution, the ground deformations, and the frictional state in the fault.

The 2D numerical model assumes a state of plane strains and that these can be considered infinitesimal. The former also considers the ground a homogeneous linear poroviscoelastic medium.

The linear elastic properties of the homogeneous material considered are the modulus of elasticity and Poisson's ratio.

The governing differential equations comprise the internal equilibrium of the solid, the fluid flow, and the storage equations.

The linear-poroelasticity theory equations are the linear constitutive relations of the porous medium, the internal equilibrium equations, and the mass balance equations in the fluid. The set of equations describes the coupling between the fluid flow and the elastic mechanical response of the porous medium. Those assume the principle of effective stresses, which relates the intergranular forces in the solid skeleton and the pore pressure, p, through the Biot-Willis parameter, α_B. By considering positive both, the tensile stresses and pore pressures greater than atmospheric, this principle reads:

$$\sigma_{ij} = \sigma'_{ij} - \alpha_B p \delta_{ij}. \quad (1)$$

Terzaghi first formulated this principle with $\alpha_B = 1$. In the above equation σ_{ij} are the total stresses, wheras δ_{ij} is the Kronecker Delta, and σ'_{ij} are the effective stresses, defined by.

$$\sigma'_{ij} = \lambda \varepsilon_v + 2G\varepsilon_{ij}. \quad (2)$$

Preprints (www.preprints.org) | NOT PEER-REVIEWED | Posted: 3 August 2022 doi:10.20944/preprints202208.0092.v1

where λ is the Lamé constant, ε_v is the volumetric deformation of the porous material, and G is the shear modulus of the porous medium, and ε_{ij} are the strain components.

Biot (1941) first proposed the classic theory of linear poroelasticity; Rice and Cleary (1976) extended its formulation and posed solving in a coupled manner the evolution of pore pressure, p, rock deformation, and friction at the fault contact [23]. The Biot equations of poroelasticity for the quasi-static case (i.e., the fluid accelerations and the relative velocity between fluid and solid are disregarded) are as follows (storativity equation):

$$\rho_f S_\varepsilon \frac{\partial p}{\partial t} + \rho_f \alpha_B \frac{\partial \varepsilon_v}{\partial t} = \nabla \cdot \left(\rho_f \frac{k}{\eta_f} (\nabla p - \rho_f g) \right). \quad (3)$$

In this equation:

- ρ_f is the fluid (water) density.
- S_ε is the constrained specific storage coefficient, and represents the volume of water either extracted from or added to storage in a confined aquifer per unit area of aquifer per unit decline or increase in the piezometric head. This unknown coefficient needs to be estimated through a model calibration. When the solid phase consists of a single constituent, the constrained specific storage becomes [24, 25]:

$$S_\varepsilon = \phi \chi_f + (\alpha_B - \phi)\chi_s = \phi \chi_f + \frac{(\alpha_B - \phi)(1 - \alpha_B)}{K} \quad (3)$$

This study considers the canonical case with $\alpha_B = 1$, then the storage coefficient S_ε is directly related to the fluid compressibility χ_f since S_ε becomes $S_\varepsilon = \phi \chi_f$.

- k is the specific permeability of the porous medium.
- η_f is the dynamic viscosity of the fluid.
- g is the gravity acceleration.

Besides, the system departs from an initial equilibrium state, in which the tectonic boundary forces, the gravity load, and the hydrostatic pressures are balanced. For simplicity, the model performs a dynamic analysis, i.e., including the inertial terms in the time response.

3. Numerical model setup

We have calibrated a simplified final model which, when subjected to the average deformations of the interseismic period, finally reaches rupture. The method helps explain the fault slip during the Andalusian earthquake and the pore pressure evolution within the medium and on the free surface.

3.1. The fault frictional model

The fault frictional constitutive law accounts for the relative slip between both edges. The fault is initially at rest, so the acting shear stresses are lower than the shear strength of the fault contacts, τ_f. Fault reactivation occurs when the effective normal-stress changes cause the acting shear stresses to reach the frictional resistance at any fault point. The Mohr-Coulomb law controls this issue:

$$\tau^* = c - \mu \sigma_n' + \xi V. \quad (4)$$

In the above equation:

- τ^* is the shear resistance at any fault point.
- c is the cohesion term of the resistance, neglected in this study.
- We include a radiation damping term that acts as a velocity-dependent cohesion, ξV, in the definition of fault strength to resolve the rupture dynamics. Then we consider a damping factor $\xi = G/3.6C_s$, with $C_s = \sqrt{G/\rho_b}$ being the shear wave speed, ρ_b the bulk rock density, $\rho_b = \phi \rho_f + (1 - \phi)\rho_d$, and ρ_d the dry rock density. The phenomenon of radiation damping accounts for the volumetric dissipation mechanism of

Preprints (www.preprints.org) | NOT PEER-REVIEWED | Posted: 3 August 2022 doi:10.20944/preprints202208.0092.v1

seismic waves, in the form of a velocity-dependent cohesion, in the definition of the friction resistance of the fault [23, 26, 27].

- μ is the friction coefficient of the contact.
- σ_n' is the effective contact (normal) pressure at any fault contact point. It is given by $\sigma_n' = p - T_n$, with T_n being the contact pressure between the fault edges (compressive pressures are positive). Its value is chosen as the maximum on both sides of the fault, $p = max(p^-, p^+)$ [28]. The fault remains locked when the shear stress acting on the fault, τ, is lower than the frictional strength, $\tau < \tau_f$; otherwise, it slips.

Besides, we assume a slip-weakening friction law for the fault, i.e., the friction coefficient value decays upon fault reactivation. So the friction coefficient shifts from the at-rest conditions, i.e., its static value, $\mu_s = 0.55$, to the dynamic value, $\mu_d = 0.5$, after a distance $D_c = 0.01\ m$, i.e., the critical slip weakening distance —a property of the fault's friction law— [13].

The numerical model assumes that the fault is rather transversely permeable, whose hydraulic flow $[kg/m^2 s]$ between its edges is simplified by a transverse permeability coefficient of $T_f = 10^{-11}\ s/m$. We model flow across the fault through a simple mass flux exchange between the two contact surfaces defining the fault. Denoting by $p \pm$ the pressures on either side of the fault and by $q_{in}^{\pm}$ the inward mass fluxes per unit area, we approximate the latter through an effective fault transmissibility, T_f, as

$$q_{in}^- = T_f(p^+ - p^-), \quad q_{in}^+ = T_f(p^- - p^+).$$

The above jump condition couples the pore pressures on both sides of the fault, allowing a transition from essentially no-flow $(T_f \to 0)$ towards pressure continuity $(T_f \to \infty)$ as T_f increases.

3.2. The ground model and properties

A battery of simulations with diverse configurations has been performed to calibrate the numerical model. The necessary confinement stresses are applied to the vertical edges so that the system is in static equilibrium at the beginning of the seismic cycle, which encompasses the corresponding stress state plus the natural settlements of the ground due to consolidation (Figure 5).

To calibrate the model, various parameters are varied, such as the porosity ϕ of the medium, variable with depth between 1% and 5%, and the intrinsic permeability, linearly decreasing with depth, ranging between $10^{-11}\ m^2$ (free surface) and $10^{-11}\ m^2$ (bottom).

The elastic modulus of the porous medium is estimated to be around $E = 20\ GPa$, its Poisson's ratio is $\nu = 0.25$, and its dry density is $\rho_d = 2.5\ T/m^3$.

We assume that the porous medium is viscoelastic, according to the Kelvin-Voigt formulation, with a viscosity coefficient of $10^7\ Pa.s$. The Biot Willis coefficient value is $\alpha_B = 1$, so there is full coupling between pore pressure variations and the deformability of the porous medium [29]. The dynamic viscosity of pore water value is $\eta_f = 10^{-3}\ Pa.s$, and its compressibility is $\chi_f = 4 \times 10^{-10}\ Pa^{-1}$.

3.3 The finite element domain

The domain is a 1-meter-thick rectangle with a depth of 20 km and a length of 28 km (Figure 5). The initial stress state includes a non-uniform distribution due to its tectonic history.

The minimum element size is 4m along the fault zone. The interpolation functions are quadratic for displacements and linear for pressures.

Preprints (www.preprints.org) | NOT PEER-REVIEWED | Posted: 3 August 2022 doi:10.20944/preprints202208.0092.v1

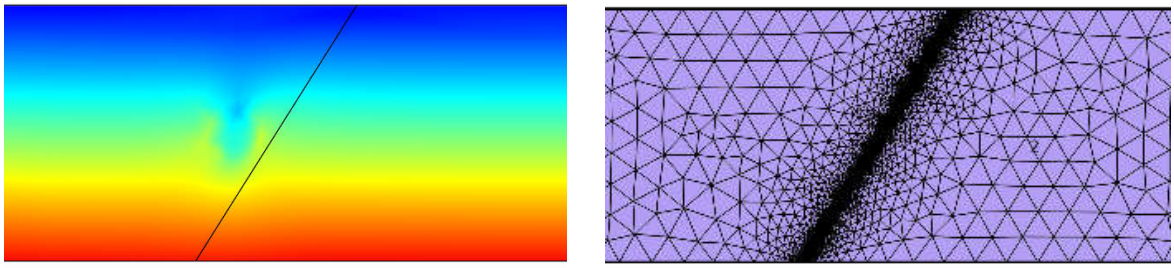

(**a**) Initial static stress state. Includes an alteration due to the tectonic history.

(**b**) Finite element mesh of the 2D plane deformation model.

Figure 5. State of initial stresses (von Mises) at the beginning of the interseismic period (left) and discretization of the finite element mesh (right).

4. Results and discussion

The conceptual model developed includes the most significant phenomena that may have led to the seismic event. This study has simplified the complexity of features arising from ground heterogeneity and the number of faults. Thus, the fault more likely to slide has been modeled. Indeed, the target zone is the area near the hypocenter to capture the seismic rupture.

In the pre-seismic phase, before the slip, the south zone of the fault is compressed by the effect of both the normal fault activity and the pushing lower detachment, which also compresses the ground. Conversely, the opposite occurs in the valley area, northward of the fault, since the zone is under tension and the pores are saturated.

In the co-seismic phase, once the fault shear resistance is reached triggering the earthquake, the valley area sinks and shrinks, closing the previously open pores and expelling the water, thus originating new sources and other hydrogeological alterations. The results of this study simulate these described effects in a similar way to what happened.

The drawback of this type of retrospective study is the lack of good estimates for the model parameters. Indeed, their values have to be adjusted so that the results obtained are as similar as possible to the effects observed, for example, settlements or elevations, the surge and loss of springs and streams, among others.

Figure 6 illustrates the earthquake patch (a) and the overpressures induced by the fault instability and the time of rupture.

Figure 7 features the patch growth in terms of fault-tangential slip velocities (a) and relative displacements between edges (b).

The simulation yields that the patch size becomes nearly 9024 m, with an average relative slip of 0.2181 m, yielding a scalar seismic moment per unit thickness is $M_0 = 1.0257 \times 10^{17}\ J$.

Preprints (www.preprints.org) | NOT PEER-REVIEWED | Posted: 3 August 2022 doi:10.20944/preprints202208.0092.v1

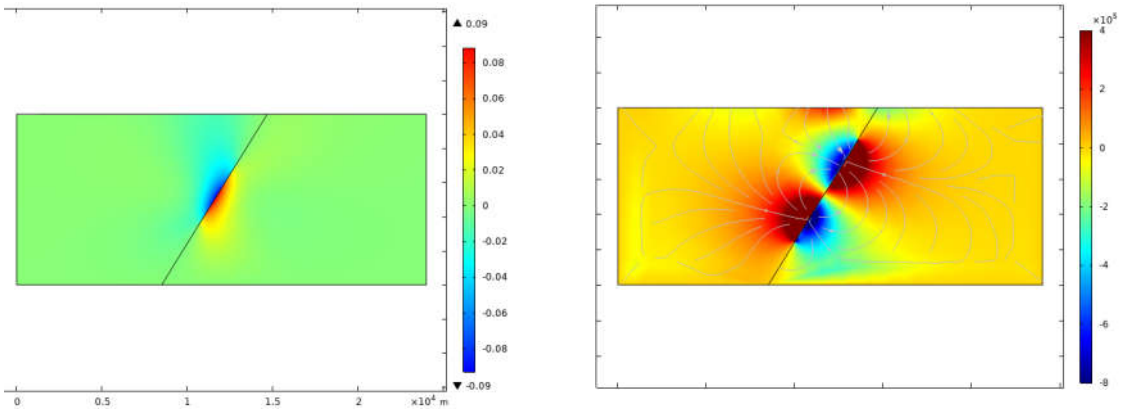

(**a**) Acceleration field at the time of rupture (**b**) Pore overpressures at the end of rupture

Figure 6. Results from the dynamic analysis: (**a**) Total acceleration field (m/s^2); (**b**) Maximum pore overpressure (Pa) induced by the earthquake.

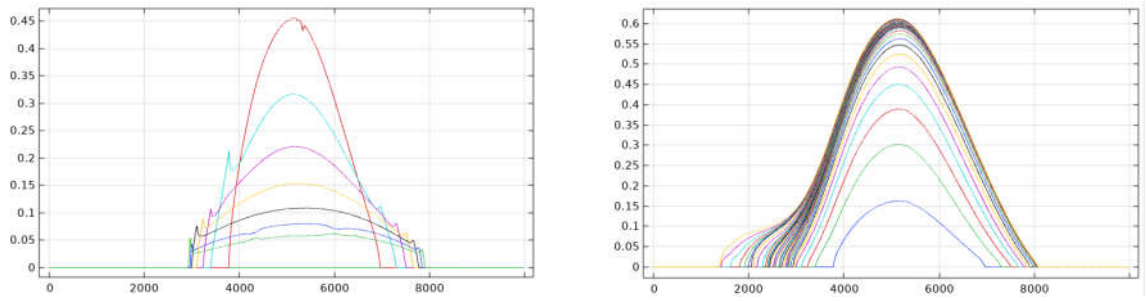

(**a**) Slip velocities (**b**) Relative slip between fault edges

Figure 7. Time progress of the earthquake rupture: the patch grows in size and accelerates during rupture. Abscissae represents the fault line. (**a**) Velocities tangent to the fault plane (m/s); (**b**) Relative slip between fault edges (m) induced during the earthquake rupture.

5. Conclusions

The implemented conceptual model is valid to explaining the event that occurred in 1884. Undoubtedly, this model would lead to more accurate results if additional field data were available, such as regional stress fields, folding issues, and hydrostatic/water pressure data, geomechanical conditions in the vicinity of the hypocenter, among others.

On the one hand, this simplified methodology helps to understand the role that pore pressure plays in triggering the earthquake. The influence of the fluid pressure field in earthquake rupture is not negligible, as pore pressure variations induce changes in the effective normal stresses on the fault, thus may leading to exceed its shear resistance. When the fault stress state is close to the critical equilibrium configuration, changes in pore pressures can trigger the fault reactivation.

On the other hand, the application of this type of models is transversal: it can provide better knowledge of the Spanish National Earthquake Catalog. Indeed, the collection of records of the hydrogeological alterations produced by historical earthquakes may supply a practical information to understand better the conceptual models and calibrate simulation models. Hence, These models can help us understand how seismicity and hydrogeological alterations seldom occur.

6. Patents

Not applicable.

Author Contributions: Conceptualization, E.S. and J.C.M.; methodology, E.S. and J.C.M.; software, M.M.H.; validation, M.M.H. and J.C.M.; formal analysis, E.S., M.M.H. and J.C.M; investigation, E.S. and J.C.M.; resources, E.S.; data curation, J.C.M. and M.M.H..; writing—original draft preparation, E.S., M.M.H. and J.C.M.; writing—review and editing, J.C.M.; visualization, J.C.M.; supervision, E.S., M.M.H. and J.C.M.; project administration, M.M.H. and E.S; funding acquisition, E.S., M.M.H. and J.C.M.. All authors have read and agreed to the published version of the manuscript."

Funding: This research was funded by the Universidad Politécnica de Madrid through the Educational Innovative Programme 2021–2022, Project codes IE22-0403.

Data Availability Statement: The data presented in this study are available from the authors upon request.

Acknowledgments: The authors gratefully thank the professors Sandro Andrés, Luis Cueto-Felgueroso and David Santillán for their technical support in the software implementations.

Conflicts of Interest: The authors declare no conflict of interest.

References

1. Quidam, U. (1885) Cartas desde los sitios azotados por los terremotos de Andalucía. Lib. Nac. y Ext. Madrid, 142. Available at: https://digibug.ugr.es/bitstream/handle/10481/7943/c-019-036%20%2837%29.pdf?sequence=1&isAllowed=y
2. Lasala y Collado, F. (1888). Memoria del comisario regio para la reedificación de los pueblos destruidos por los terremotos en las provincias de Granada y Málaga. M. Minuesa de los Ríos, Impresor, Madrid. Available at: http://www.bibliotecavirtualdeandalucia.es/catalogo/es/catalogo_imagenes/grupo.do?path=150661
3. Fouqué, F. (1889). Estudios referentes al terremoto de Andalucía ocurrido el 25 de diciembre de 1884 ya la constitución geológica del terreno conmovido, hecho por la comisión destinada al objeto por la Academia de Ciencias de París.
4. Botella y Hornos, F. (1885). Los terremotos de Málaga y Granada. Bol. Soc. Geográfica de Madrid, t. XVII, 30.
5. Fernández de Castro, M., Lasal, J. P., Cortazar, D., & Tarín, J. G. (1885). Terremotos de Andalucía. Informe de la Comisión nombrada para su estudio dando cuenta del estado de los trabajos en 7 de marzo de 1885.
6. Comisión Italiana. (1886). Informe del terremoto de Andalucía de 1884. R. Accademia dei Lincei. Memorie della classe di scienze fisiche, matematiche e naturalli. Volume III, 195 y mapas.
7. Seco de Lucena, L. (1941): Crónicas sobre el terremoto de Andalucía de 1884. Memorias. 79-103.
8. Wang, Chi-Yuen, and Michael Manga. "Temperature and Composition Changes." Earthquakes and Water. Springer, Berlin, Heidelberg, **2010**. 97-115.
9. Santillán, D., Sanz de Ojeda, A., Cueto-Felgueroso, L.; Mosquera, J. C. Sismicidad inducida en embalses. Una aproximación mediante un modelo conceptual. Hidrogeología: Retos y experiencias, UIMP, Madrid (Spain), **2018**.
10. Fernández-García, C.; Ruano, P. Caracterización de la geometría del Polje de Zafarraya a partir de prospección gravimétrica (Cordillera Bética). *Geogaceta*, **2016**.
11. de Galdeano, C.S. The Zafarraya Polje (Betic Cordillera, Granada, Spain), a basin open by lateral displacement and bending. *Journal of Geodynamics*, **2013**, 64, 62-70.
12. López Chicano, M.; Pulido-Bosch, A. Síntesis hidrogeológica de los acuíferos de Sierra Gorda, Polje de Zafarraya y Hacho de Loja. Libro Homenaje a Manuel del Valle Cardenete. Aportaciones al conocimiento de los acuíferos andaluces. IGME, CHG, IAA (COPTJA), Diputación Provincial de Granada, Madrid, **2002**, 311-340.
13. Bizzarri, A. How to promote earthquake ruptures: Different nucleation strategies in a dynamic model with slip-weakening friction. *Bulletin of the Seismological Society of America*, **2010**, 100(3), 923-940.
14. Srivastava, S. P., Schouten, H., Roest, W. R., Klitgord, K. D., Kovacs, L. C., Verhoef, J., & Macnab, R. Iberian plate kinematics: a jumping plate boundary between Eurasia and Africa. *Nature*, **1990**, 344(6268), 756-759.
15. Galindo-Zaldívar, J., Gil, A. J., Borque, M. J., González-Lodeiro, F., Jabaloy, A., Marín-Lechado, C., ... & Sanz de Galdeano, C. Desarrollo simultáneo reciente de pliegues y fallas en las Cordilleras Béticas: la Falla de Zafarraya y el Pliegue de Sierra Tejeda. *Geo-Temas*, **2004**, 6, 147-150.
16. Reicherter, K. R., Jabaloy, A., Galindo-Zaldívar, J., Ruano, P., Becker-Heidmann, P., Morales, J., ... & González-Lodeiro, F. Repeated palaeoseismic activity of the Ventas de Zafarraya fault (S Spain) and its relation with the 1884 Andalusian earthquake. *International Journal of Earth Sciences*, **2003**, 92(6), 912-922.
17. Reicherter, K. R.; Peters, G. Neotectonic evolution of the central Betic Cordilleras (southern Spain). Tectonophysics, **2005**, 405(1-4), 191-212.
18. Muñoz, D.; Udías, A. (**1981**). El Terremoto de Andalucía del 25 de diciembre de 1884. IGN. Available online: http://www.ign.es/web/resources/sismologia/publicaciones/Andalucia1884.pdf
19. López Chicano, M.; Pulido-Bosch, A. Síntesis hidrogeológica de los acuíferos de Sierra Gorda, Polje de Zafarraya y Hacho de Loja. Libro Homenaje a Manuel del Valle Cardenete. Aportaciones al conocimiento de los acuíferos andaluces. IGME, CHG, IAA (COPTJA), **2002**, Diputación Provincial de Granada, Madrid, 311-340.
20. López-Chicano, M. Contribución al conocimiento del sistema hidrogeológico kárstico de Sierra Gorda y su entorno (Granada y Málaga) (Doctoral dissertation, Universidad de Granada), **1993**.

 doi:10.20944/preprints202208.0092.v1

21. López Arroyo, A., Martín Martín, A. J.; Mezcua Rodríguez, J. Terremoto de Andalucía. Influencia en sus efectos de las condiciones del terreno y del tipo de construcción. El terremoto de Andalucía de 1884, **1980**, 5-94.
22. Udías, A.; Muñoz, D. The Andalusian earthquake of 25 December 1884. *Tectonophysics*, **1979**, 53(3-4), 291-299.
23. Cueto-Felgueroso, L., Santillán, D.; Mosquera, J.C. Stick-slip dynamics of flow-induced seismicity on rate and state faults. *Geophysical Research Letters*, **2017**, 44(9), 4098-4106.
24. Coussy, O. Poromechanics. John Wiley & Sons, London, **2004**.
25. Verruijt, A. Theory and problems of poroelasticity. **2013**, Delft University of Technology, 71.
26. Rice, J.R. Spatio-temporal complexity of slip on a fault, *J. Geophys. Res*., **1993**, 98, 9885–9907.
27. Lapusta, N.; Rice. J.R. Nucleation and early seismic propagation of small and large events in a crustal earthquake model, *J. Geophys. Res*. **2003**, 108, B42205, doi:10.1029/2001JB000793.
28. Jha, B.; Juanes, R. Coupled multiphase flow and poromechanics: A computational model of pore pressure effects on fault slip and earthquake triggering. *Water Resources Research*, **2014**, 50(5), 3776-3808.
29. Rice, J. R.; Cleary, M. P. Some basic stress diffusion solutions for fluid-saturated elastic porous media with compressible constituents. *Reviews of Geophysics*, **1976**, 14(2), 227-241.